



UNIVERSITY OF LEEDS

This is a repository copy of *Coupled-coherent-states approach for high-order harmonic generation*.

White Rose Research Online URL for this paper:  
<http://eprints.whiterose.ac.uk/88788/>

Version: Accepted Version

---

**Article:**

Symonds, C, Wu, J, Ronto, M et al. (3 more authors) (2015) Coupled-coherent-states approach for high-order harmonic generation. *Physical Review A*, 91 (2). 023427. ISSN 1050-2947

<https://doi.org/10.1103/PhysRevA.91.023427>

---

**Reuse**

Unless indicated otherwise, fulltext items are protected by copyright with all rights reserved. The copyright exception in section 29 of the Copyright, Designs and Patents Act 1988 allows the making of a single copy solely for the purpose of non-commercial research or private study within the limits of fair dealing. The publisher or other rights-holder may allow further reproduction and re-use of this version - refer to the White Rose Research Online record for this item. Where records identify the publisher as the copyright holder, users can verify any specific terms of use on the publisher's website.

**Takedown**

If you consider content in White Rose Research Online to be in breach of UK law, please notify us by emailing [eprints@whiterose.ac.uk](mailto:eprints@whiterose.ac.uk) including the URL of the record and the reason for the withdrawal request.



[eprints@whiterose.ac.uk](mailto:eprints@whiterose.ac.uk)  
<https://eprints.whiterose.ac.uk/>

# Coupled coherent state approach for high-order harmonic generation

C. Symonds,<sup>1</sup> J. Wu,<sup>2</sup> M. Ronto,<sup>1</sup> C. Zagoya,<sup>2</sup> C. Figueira de Morisson Faria,<sup>2</sup> and D. V. Shalashilin<sup>1</sup>

<sup>1</sup>*School of Chemistry, University of Leeds, Leeds LS2 9JT, United Kingdom*

<sup>2</sup>*Department of Physics and Astronomy, University College London,  
Gower Street, London WC1E 6BT, United Kingdom*

In this paper we report a version of the Coupled Coherent States (CCS) method which is able to accurately compute the HHG spectrum of an electron in a laser field in one dimension by the use of trajectory-guided grids of Gaussian wavepackets. It is shown that by periodic re-projection of the wavefunction and dynamically altering the basis set size, the method can account for a wavefunction which spreads out to cover a large area in phase space while still keeping computational expense low. The HHG spectra obtained show good agreement with those from a time dependent Schrödinger equation solver. We show also that the part of the wavefunction which is responsible for HHG moves along a periodic orbit which is far from that of classical motion. Although this paper is a proof of principle and therefore focussed on a simple one-dimensional system, future generalisations for the multi-electron case are discussed.

PACS numbers: 33.20.Xx, 42.50.Hz

## I. INTRODUCTION

High-order harmonic generation (HHG) is a phenomenon in which matter responds highly non-linearly to an input near-infrared field, generating high-frequency radiation up to the extreme ultraviolet regime [1]. This phenomenon has a wide range of applications, such as coherent light sources in the extreme ultraviolet [2–4] and soft x-ray [5–7] frequency range, attosecond ( $10^{-18}$  s) pulse generation [8–10], and attosecond molecular imaging [11, 12]. HHG can be explained by means of the well-known semi-classical three-step model [13–16] or equally well by the fully quantum version given by Lewenstein *et al.*[17]. The three step model splits the process into three distinct stages; firstly an electron tunnels through the barrier formed by the Coulomb potential and the laser field, then oscillates and gains kinetic energy under the influence of the laser field before finally being pulled back to recombine with the parent ion when the laser field inverts its direction, resulting in the emission of a harmonic photon. Both experimental and theoretical studies have shown that this process produces a spectrum which has a typical character, decreasing rapidly for the first few harmonics, then exhibiting a broad plateau before ending with a sharp cut-off. This cut-off is related to the maximal kinetic energy the electron has upon return, and this kinetic energy is itself related to the ponderomotive energy  $U_P$ , which for a monochromatic driving field is given by  $U_P = \mathcal{E}_0^2/4\omega_0^2$  where  $\mathcal{E}_0$  and  $\omega_0$  are respectively the laser field intensity and frequency. If the electron starts from the core and is acted on by a monochromatic field, this kinetic energy is equal to  $3.17 U_P$ .

At present, several theoretical approaches have been established to compute HHG spectra. The numerical solution of the time-dependent Schrödinger equation contains no physical approximations and is straightforward for one-dimensional, one-electron systems [18, 19],

but as the numerical effort increases exponentially with the number of degrees of freedom, it is not applicable to a three-dimensional complex system. This is a serious obstacle towards modelling correlated multi-electron dynamics in the attosecond regime, which are important as these dynamics play a major role in many strong-field phenomena such as, for example, electron migration and attosecond hole creation (for a review see, e.g., [20] and references therein). Furthermore, as it lacks the clarity of an orbit-based picture it is difficult to define a physical interpretation using this method. One may however employ semi-analytical approaches such as the strong field approximation (SFA). The SFA underlies many of the current analytical approaches to HHG and also other strong-field phenomena such as above-threshold ionisation (ATI) or non-sequential double ionisation (NSDI), providing a transparent physical picture for quantum interference in these phenomena [21–23]. When using the SFA however, the laser field is neglected when the electrons are bound to atoms or molecules, the Coulomb potential is neglected when the electrons are in the continuum, and the internal atomic structure is over simplified. In particular, approximating the continuum by field-dressed plane waves poses serious difficulties when the interplay between the Coulomb potential and the external field becomes important such as is the case for the prominent low-frequency structure [24–27] and fan-shaped interference pattern [28, 29] in ATI, or for NSDI in circularly polarised fields [30, 31]. Recently, Coulomb-corrected analytical approaches have been developed and successfully applied to strong field phenomena [24, 32–34]. These approaches however require the external field to be dominant.

In light of the above problems, an alternative method is desirable which is orbit-based, but makes no simplifications on the target/binding potential. One such alternative is the Coupled Coherent States (CCS) method [35–39]. This method allows the simulation

of multidimensional many-body quantum dynamics by projecting the wavefunction onto a basis of trajectory-guided coherent states coupled through time propagation equations. The trajectories along which the wavefunction is propagated are not guided by a classical potential unlike in some other trajectory guided methods (mainly semi-classical in nature), but instead are guided by a quantum average over the guiding coherent states. This incorporates corrections into the potential, accounting for such effect as zero point energy and resulting in a shallower potential after the fashion of [40]. As such, the CCS equations describe a method which is, in principle, formally exact and is capable of simulating non-classical events such as quantum interference effects [35] and multidimensional tunnelling [37]. A variation of the CCS method has also been applied successfully in the strong field context [41]. In phenomena for which coherence is important however there exists a major challenge to overcome, namely that as the wavefunction propagates in phase space the interference may not be accurately represented by a small CCS basis. This happens due to the fact that at longer times trajectories can misguide the basis, making propagation less and less accurate.

In this article we endeavour to address these concerns, and to show that with simple technical modifications to the standard CCS method, the generation of HHG spectra can be achieved giving a good agreement with spectra generated by use of the time-dependent Schrödinger equation. A similar version of the CCS method to that reported here has been used previously in Ref. [42] for the study of quantum dynamics in phase space. In Section II we provide the necessary theory in order to understand our results including an overview of the CCS method and its governing equations (sections II A and II B), a description of the theoretical model used to show the efficacy of the CCS method for generating HHG spectra (section II C) and a description of the necessary modifications made to the CCS method in order to model this system (section II D). In section III we present the results of our simulation. Since the CCS method models quantum mechanics in phase space our numerical experiment can be visualised in terms of an orbit which the part of the wavefunction responsible for HHG follows. We show that this orbit is very different from that of classical mechanics. In section IV we draw our conclusions and discuss the possibility of using CCS with modifications suggested in this paper for accurate description of multi-electron systems.

## II. THEORY

### A. Coupled Coherent States

In the CCS method a wavefunction is represented as a superposition of trajectory guided coherent states. In the coordinate representation, these one-dimensional coherent

states are Gaussian wavepackets [43] centred at position  $q$  with momentum  $p$  which can be expressed in the form

$$\langle x|z\rangle = \left(\frac{\gamma}{\pi}\right)^{\frac{1}{4}} \exp\left(-\frac{\gamma}{2}(x-q)^2 + \frac{i}{\hbar}p(x-q) + \frac{ipq}{2\hbar}\right). \quad (1)$$

These coherent states are eigenstates of the annihilation operator such that

$$\begin{aligned} \hat{a}|z\rangle &= z|z\rangle \\ \langle z|\hat{a}^\dagger &= \langle z|z^* \end{aligned} \quad (2)$$

where  $\hat{a}$  and  $\hat{a}^\dagger$  are the annihilation and creation operators respectively, and hence

$$\begin{aligned} z &= \left(\frac{\gamma}{2}\right)^{\frac{1}{2}} q + \frac{i}{\hbar} \left(\frac{1}{2\gamma}\right)^{\frac{1}{2}} p \\ z^* &= \left(\frac{\gamma}{2}\right)^{\frac{1}{2}} q - \frac{i}{\hbar} \left(\frac{1}{2\gamma}\right)^{\frac{1}{2}} p \end{aligned} \quad (3)$$

where  $\gamma$ , the coherent state width parameter can be assumed to be unchanging with a value of  $\gamma = m\omega/\hbar$  where  $m$  is the particle mass and  $\omega$  is the interior frequency, and as calculations are in atomic units it is assumed that  $m = \omega = 1$ , and also  $\hbar = 1$ .

The coherent states can be used to construct a non-orthogonal basis where the basis vectors have a non-zero overlap given by

$$\langle z'|z\rangle = \exp\left[z^*z - \frac{z'^*z'}{2} - \frac{z^*z}{2}\right] \quad (4)$$

and act upon the Hamiltonian of a system such that

$$\langle z'|\hat{H}|z\rangle = \langle z'|z\rangle H_{\text{ord}}(z'^*, z) \quad (5)$$

with  $H_{\text{ord}}(z'^*, z)$  being the classical analogue of the normally ordered Hamiltonian  $\hat{H}^{\text{ord}}(\hat{a}^\dagger, \hat{a})$  in which the powers of  $\hat{a}^\dagger$  precede those of  $\hat{a}$ , as can be seen by consideration of equation (2). Equation (5) is simply a way to find  $\langle z'|\hat{H}|z\rangle$  by integration, and the use of the ordered Hamiltonian in this greatly simplifies the equations in some cases.

It should be noted that the equations as they have been given are one-dimensional in nature and multi-dimensional coherent states can be shown as products of  $M$  one-dimensional states such that

$$|\mathbf{z}_k(t)\rangle = \prod_{m=1}^M |z_k^{(m)}(t)\rangle. \quad (6)$$

In the CCS method, the wavefunction is given in terms of a finite sum of these coherent states each with a quantum amplitude such that

$$\begin{aligned} |\Psi(t)\rangle &= \sum_{k=1, N} |\psi_k(t)\rangle \\ &= \sum_{k=1, N} A_k(t) |\mathbf{z}_k(t)\rangle \end{aligned} \quad (7)$$

for a finite set of  $N$  bases where the fast oscillating amplitude  $A_k(t)$  is chosen such that  $|\Psi(t)\rangle$  is normalised over all  $k$  and can be split into a smooth pre-exponential factor and the classical action such that

$$A_k(t) = D_k(t)e^{iS_k(t)} \quad (8)$$

where the action  $S_k$  is given by

$$S_k(t) = \int \left[ i \frac{\dot{\mathbf{z}}_k(t) \mathbf{z}_k^*(t) - \mathbf{z}_k(t) \dot{\mathbf{z}}_k^*(t)}{2} - \langle \mathbf{z}_k(t) | \hat{H} | \mathbf{z}_k(t) \rangle \right] dt. \quad (9)$$

The initial values for the  $D_k(0)$  pre-factors arise from the discretised identity formula

$$\mathbb{I} = \sum_{j,k=1,N} |\mathbf{z}_j(t)\rangle \Omega_{jk}^{-1} \langle \mathbf{z}_k(t)| \quad (10)$$

where  $\Omega^{-1}$  is the inverse of the overlap matrix  $\Omega$  with elements

$$\Omega_{jk} = \langle \mathbf{z}_j(t) | \mathbf{z}_k(t) \rangle = \prod_{m=1}^M \langle z_j^{(m)}(t) | z_k^{(m)}(t) \rangle. \quad (11)$$

By applying this identity to the initial wavefunction  $|\Psi(0)\rangle$  at time  $t = 0$ ,

$$\begin{aligned} |\Psi(0)\rangle &= \mathbb{I} |\Psi(0)\rangle \\ &= \sum_{j,k=1,N} |\mathbf{z}_j(0)\rangle \Omega_{jk}^{-1} \langle \mathbf{z}_k(0) | \Psi(0) \rangle \\ &= \sum_{j=1,N} D_j(0) |\mathbf{z}_j(0)\rangle \end{aligned} \quad (12)$$

If then an amplitude  $C_k(0) = \langle \mathbf{z}_k(0) | \Psi(0) \rangle$  is defined then the initial values in the vector  $D_j$  can be found by solving the system of linear equations

$$C_k(0) = \Omega_{jk} D_j(0). \quad (13)$$

## B. Dynamics Equations for the CCS method

Dynamics in the CCS method for a particular basis function  $|\psi_k(t)\rangle$  are determined by the time propagation equations for the action  $S_k$ , the coherent state  $|\mathbf{z}_k\rangle$  and the smooth pre-exponential factor  $D_k$ . The equations governing this are calculated more fully in previous publications, for example [38], but a brief overview is given here.

The time propagation equation for  $z_k$  is calculated using the single configurational Lagrangian

$$\mathcal{L}_k = \left\langle \psi_k(t) \left| i \frac{\partial}{\partial t} - \hat{H} \right| \psi_k(t) \right\rangle. \quad (14)$$

By applying Hamilton's equations to this Lagrangian it can be found that

$$i\dot{z}_k = \frac{\partial H_{\text{ord}}(z_k^*, z_k)}{\partial z_k^*}. \quad (15)$$

The coupling between the coherent states is governed by the time propagation equations for the pre-exponential factor  $D_k$ , and as such the time derivative equations are calculated from the complete wavefunction  $|\Psi(t)\rangle$ . While the equation for  $\dot{D}_k$  can be calculated by use of the variational principle, a much simpler derivation is possible by use of the time dependent Schrödinger equation. Using this method, it can be seen that for the wavefunction described by equation (7),

$$\begin{aligned} \sum_i \langle \mathbf{z}_j | \mathbf{z}_i \rangle \frac{dA_i}{dt} &= -i \sum_k \left[ \langle \mathbf{z}_j | \hat{H} | \mathbf{z}_k \rangle \right. \\ &\quad \left. - i \langle \mathbf{z}_j \left| \frac{\partial \mathbf{z}_k}{\partial t} \right\rangle \right] A_k. \end{aligned} \quad (16)$$

By using equation (8) and the relationship that

$$\langle \mathbf{z}_j | \dot{\mathbf{z}}_k \rangle = \langle \mathbf{z}_j | \mathbf{z}_k \rangle \left( \mathbf{z}_j^* \dot{\mathbf{z}}_k - \frac{\mathbf{z}_k^* \dot{\mathbf{z}}_k + \mathbf{z}_k \dot{\mathbf{z}}_k^*}{2} \right), \quad (17)$$

it is fairly straight forward to calculate that

$$\begin{aligned} \sum_i \langle \mathbf{z}_j | \mathbf{z}_i \rangle \frac{dD_i}{dt} &= \\ -i \sum_k \langle \mathbf{z}_j | \mathbf{z}_k \rangle \delta^2 H'_{\text{ord}}(z_j^*, z_k) D_k e^{i(S_k - S_j)} \end{aligned} \quad (18)$$

where

$$\begin{aligned} \delta^2 H'_{\text{ord}}(z_j^*, z_k) &= H_{\text{ord}}(z_j^*, z_k) - H_{\text{ord}}(z_k^*, z_k) \\ &\quad - i(z_j^* - z_k^*) \dot{z}_k. \end{aligned} \quad (19)$$

The coupling matrix  $\langle \mathbf{z}_j | \mathbf{z}_k \rangle \delta^2 H'_{\text{ord}}(z_j^*, z_k)$  is small and traceless as  $\delta^2 H'_{\text{ord}}(z_j^*, z_k)$  is small for coherent states close to each other, and the overlap  $\langle \mathbf{z}_j | \mathbf{z}_k \rangle$  is small for coherent states remote from each other. Equation (18) can be solved without matrix inversion as a system of linear equations for  $dD_i/dt$ , and this equation together with equations (9) and (15) make up the governing equations of the method.

The CCS theory can also be formulated in terms of a continuum over-complete basis where the identity operator in 1D is given as

$$\mathbb{I} = \frac{1}{\pi} \int d^2 z |z\rangle \langle z|. \quad (20)$$

Under these conditions, in equation (18) for the amplitudes, the sum will be replaced by an integral and (18) becomes an integro-differential equation (see [35] for more details). The continuum form of CCS theory has been used to derive various approximations such as the semi-classical Herman-Kluk theory and Heller's Frozen Gaussian Approximation [44]. Also several modifications of the CCS method exist, which include Fermionic CCS [41], Multilayer CCS [45] and the more generalised multi-configurational Ehrenfest approach [46, 47] and its *ab initio* "on the fly" version [48–50].

### C. Model

In this article, for the sake of simplicity and as only a proof of principle is required here, we consider a model where a single electron interacts with a strong laser field and consider only the motion along the principle axis of the laser field as a one-dimensional system. The Hamiltonian of such a system can be given as

$$H = \frac{p^2}{2} + V_a + V_\varepsilon \quad (21)$$

where  $V_a$  is the binding potential and  $V_\varepsilon$  is the interaction potential with the laser field in the length gauge. For simplicity, the binding potential used in this case is a 1D short range Gaussian potential  $V_G(x) = -\exp(-\lambda x^2)$  with a width of  $\lambda = 0.5$ , and the laser field interaction potential used has the form  $V_\varepsilon(x, t) = x\mathcal{E}(t) = x\mathcal{E}_0\cos(\omega_0 t)$  with intensity  $\mathcal{E}_0 = 0.1$  and frequency  $\omega_0 = 0.05$ . Using these potentials, an ordered Hamiltonian for this system can be constructed in the coherent state formalism using the  $z$ -notation such that

$$H_{\text{ord}}(z_j^*, z_k) = -\frac{\hbar^2\gamma}{4m} (z_j^{*2} + z_k^2 - 2z_j^*z_k - 1) - \sqrt{\frac{\eta}{\lambda}} \exp(-\eta\rho_{jk}^2) + \rho_{jk}\mathcal{E}(t), \quad (22)$$

where  $\rho_{jk} = (z_j^* + z_k)/\sqrt{2\gamma}$  and  $\eta = \gamma\lambda/(\gamma + \lambda)$ . As mentioned earlier, this reordering results in changes to the effective potential, giving a shallower potential than the form in coordinate representation such as that used in [42]. The kinetic energy term of the Hamiltonian is obtained through operator reordering and the potential terms through integration with equation (1). The HHG spectrum of this system is calculated from the Fourier transform of the time-dependent dipole moment  $d(t)$  which can be given in terms of a time-dependent operator  $\hat{d}(t)$

$$d(t) = \langle \Psi(t) | \hat{d}(t) | \Psi(t) \rangle \quad (23)$$

This is easily expanded out in terms of the elements of the dipole momentum matrix  $d_{jk}$  such that

$$\begin{aligned} d(t) &= \sum_{j,k} D_j^* D_k \exp(i(S_k - S_j)) \langle z_j | \hat{d}(t) | z_k \rangle \\ &= \sum_{j,k} D_j^* D_k \exp(i(S_k - S_j)) \langle z_j | z_k \rangle d_{jk}(t). \end{aligned} \quad (24)$$

The dipole moment can be expressed in length, velocity or acceleration forms [51, 52]. In the length form the dipole moment is very large in regions away from the core and hence the dynamics in these regions is over-emphasised. In the velocity form no spatial region is favoured over another. In the acceleration form however the region close to the core is probed, which is the region in which HHG occurs according to the three-step

model. Using the Heisenberg equations this acceleration form can be computed, and for the Gaussian potential this gives

$$d_{jk}(t) = \langle -\nabla \vec{V}(x) \rangle = -\left(\frac{\gamma}{\gamma + \lambda}\right)^{\frac{3}{2}} \rho_{jk} e^{-\frac{\gamma\rho_{jk}^2}{2(\gamma + \lambda)}} \quad (25)$$

where  $\rho_{jk}$  is the same as for equation (22)

### D. The Adaptive Basis Re-projection Technique

It has been usual practice in previous applications of the CCS method to construct the basis set for a CCS wavefunction from a compressed random swarm which follows a Gaussian distribution [38]. In the case considered in this article this initial distribution is unsuitable for modelling the wavefunction as a compressed basis is too localised to sufficiently describe the wavefunction fully at long times. To remedy this the wavefunction was described as a basis set corresponding to a grid in phase space with a regular spacing between grid points. This allows the initial wavefunction to be described over a much larger area in phase space. This however raised two further problems. Firstly, the dynamics of this particular system cause the trajectories to guide the wavefunction far from the initial position. This

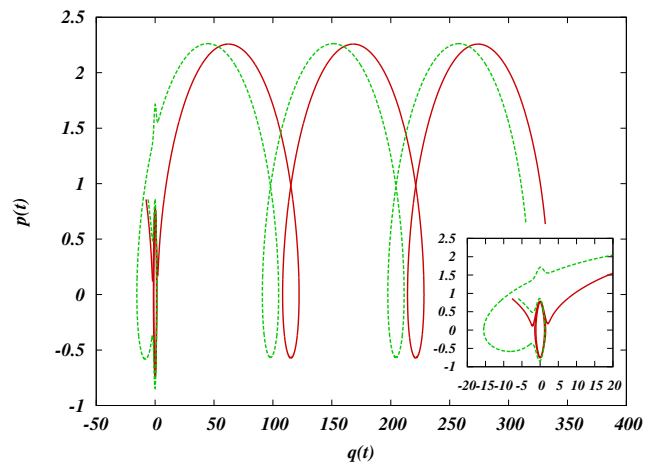


FIG. 1. The path of the trajectories initially located close to the centre of the wavefunction as they propagate through phase space. The smaller frame shows the path the trajectories take in the region close to the origin. As a result of this after a short time, approximately 20 a.u., the overlap between the wavefunction trajectories and the initial grid points becomes too small for the CCS dynamics to be accurately calculated and the coherent states lose coupling.

means that to accurately model the time evolution of the wavefunction a very large grid would be needed. Secondly a regular grid requires more trajectories to describe the wavefunction, and the larger the grid the higher the computational requirement, meaning that

past a certain grid size the computational requirements are too large for the system to be modelled effectively.

A solution to these problems can be found by using an adaptive re-projection technique. This technique serves to keep the maximum size of the grid low, needing to only describe a large enough area in phase space to account for the movement of the wavefunction over a small time  $\tau$ . A further reduction in overall computational cost of over 50% can be achieved by truncating those trajectories which do not give a large contribution to the wavefunction. Similar techniques have been used in the past to counter time restrictions in simulations using the Herman-Kluk method [53, 54], the hybrid Heller Frozen Gaussian method [55, 56], or in the phase space approach [57] with success. This technique consists of three stages:

- (i) The overlap between the wavefunction  $|\Psi(t)\rangle$  made up of  $N$  basis functions  $|\psi_k(t)\rangle$  and the initial regular grid made up of  $N_0$  grid points  $z_j^{grid}$ , separated by distances  $dq = \Delta\sqrt{\frac{2}{\gamma}}$  and  $dp = \Delta\sqrt{2\gamma}$ , is calculated to find the quantity

$$C'_j = \sum_k^N \langle z_j^{grid} | z_k(t) \rangle D_k(t) e^{iS_k(t)}, \quad (26)$$

then values of  $C'_j$  which do not satisfy the condition

$$|C'_j| \geq \zeta \quad (27)$$

are discarded, leaving  $N'$  of the initial  $N_0$  values. In equation (27),  $\zeta$  is the basis threshold parameter.

- (ii) The wavefunction is re-projected upon the initial regular grid, not including those grid points which correspond to values of  $C'_j$  which have been discarded. This is done by using a form of the identity operator in equation (10) such that

$$\begin{aligned} |\Psi(t)\rangle &= \sum_{i,j}^{N'} \sum_k^N |z_i^{grid'}\rangle \Omega_{ij}^{-1} \langle z_j^{grid'} | z_k(t) \rangle D_k(t) e^{iS_k(t)} \\ &= \sum_i^{N'} D'_i |z_i^{grid'}\rangle. \end{aligned} \quad (28)$$

As such the set of trajectories describing the wavefunction after re-projection is  $|z_i^{grid'}\rangle$  and the set of amplitudes  $D'_i$  can be calculated from the set of linear equations

$$C'_j = \Omega_{ij}^{grid'} D'_i \quad (29)$$

with the action set back to  $S'_i = 0 \forall i$

- (iii) The wavefunction is propagated for an amount of time  $\tau$  using the equations (15) and (18). The selected grid points move and exchange amplitudes, then re-projection is started again for the wavefunction  $|\Psi(t + \tau)\rangle$

It can be immediately seen that both the accuracy and computational cost of the method will increase as  $\zeta \rightarrow 0$ .

### III. RESULTS

The adaptive grid CCS technique was tested on a grid symmetrically ordered around a central point  $\mathbf{z}_0$  which was located in phase space at  $(q, p) = (0, 0)$ . The coherent state  $|\mathbf{z}_0\rangle$  is a good approximation to the ground state of the system. It was found empirically that an initial grid of  $80 \times 20$  points was sufficient to model the wavefunction, with an additional point located at  $\mathbf{z}_0$  which serves to provide additional stability. The size of the grid on the  $q$ -axis must of course account for the maximum displacement experienced by the wavefunction so as to avoid significant lost amplitude from the trajectories near the edge of the grid which would greatly affect the norm. Since for larger values of the basis threshold parameter the wavefunction is likely to be projected on fewer trajectories, these values require denser grids to adequately describe the wavefunction. The density of the grid is determined by the spacing parameter  $\Delta$  and, by choosing the value of  $\Delta$  correctly, the initial norm of the wavefunction is set very close to unity. To evaluate the quality of results, the properties of a wavefunction calculated using the CCS method was compared against those calculated using the time dependent Schrödinger equation solver, considering various values for the basis threshold parameter.

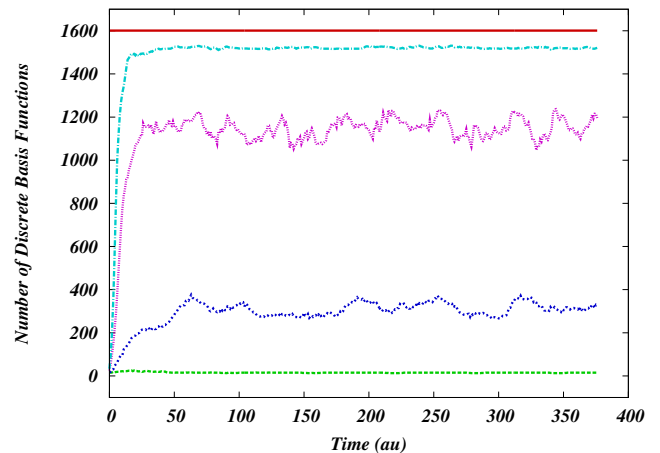


FIG. 2. Changing number of basis vectors for different values of the basis threshold parameter investigated in a logarithmic fashion. Selected values values from a range of  $\zeta = 10^{-1}$  to  $\zeta = 10^{-10}$  are given, namely  $\zeta = 10^{-1}$  (large dashed),  $\zeta = 10^{-3}$  (small dashed),  $\zeta = 10^{-5}$  (dotted) and  $\zeta = 10^{-8}$  (dot-dashed), as well as the case where  $\zeta = 0$  (solid) and so the number of basis vectors stays constant.

For  $\zeta \neq 0$ , as the system is propagated in time the wavefunction spreads out and the number of basis

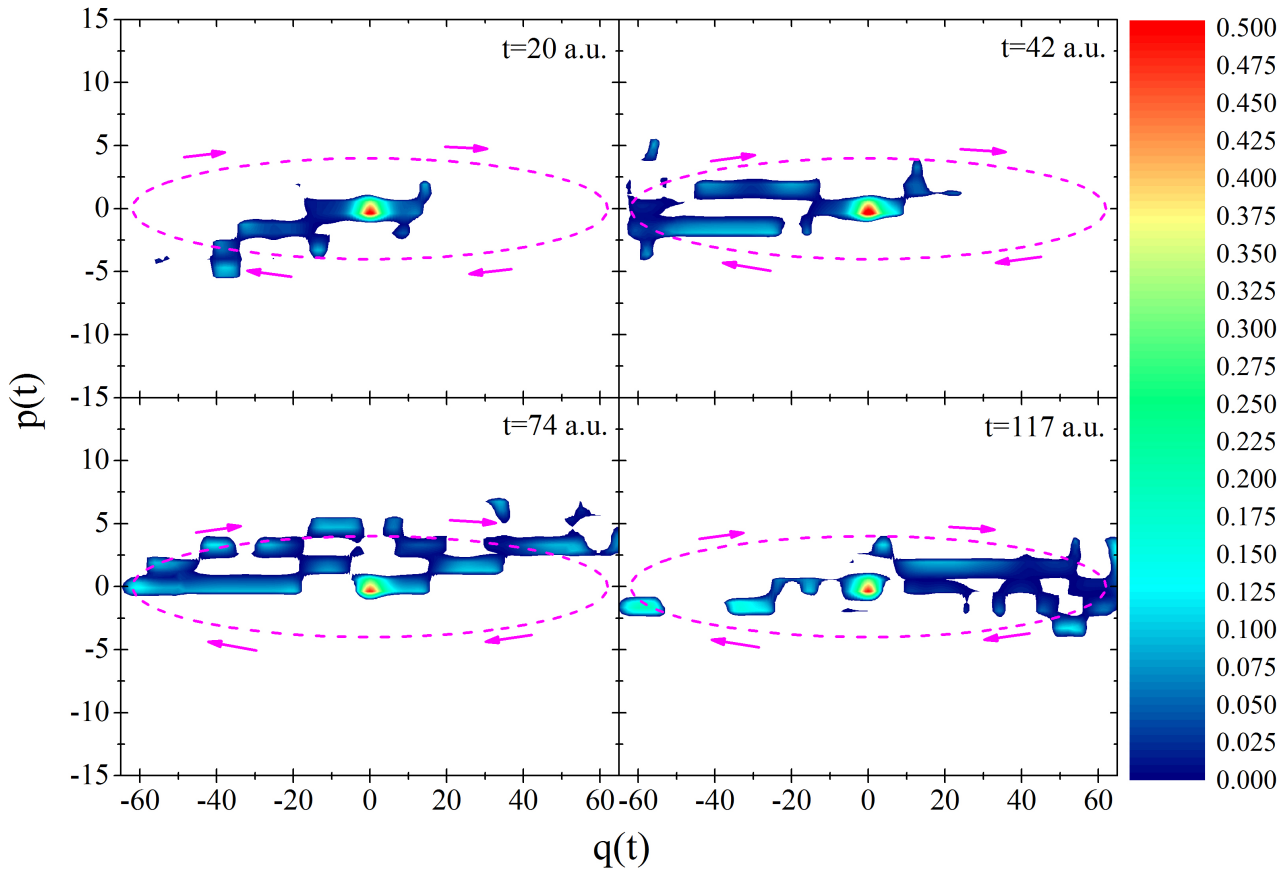


FIG. 3. Motion of the wavefunction over time on a grid of  $80 \times 20$  coherent states with a separation of  $\Delta = 1.59 \text{ a.u.}$  and with  $\zeta = 10^{-3}$ . Each pane illustrates the entire grid, with whitespace denoting areas where the gridpoints are omitted during reprojection. The panes show the motion of the important parts of the wavefunction after reprojection at  $t = 20 \text{ a.u.}$ ,  $42 \text{ a.u.}$ ,  $74 \text{ a.u.}$ , and  $117 \text{ a.u.}$ , and clearly illustrates how the external field has an effect on the wavefunction, drawing a portion of it into an elliptical motion around the core of the wavefunction. The elliptical motion of this portion of the wavefunction is illustrated by the dashed line.

vectors above the cut-off increases until it reaches a plateau value around which it stays for the duration of propagation. This can be seen in figure 2. The value at which the number of basis vectors plateaus determines how computationally expensive the simulation is, and so it is desirable to use the largest possible value of the basis threshold parameter which allows for accurate simulation of the system, referred to hereafter as the maximum effective cut-off,  $\zeta_{MEC}$ . The  $\zeta_{MEC}$  value was determined based on the agreement of the auto-correlation function (ACF) with that calculated using the TDSE solver.

As the CCS method represents the quantum dynamics in phase space, the motion of the wavefunction can easily be visualised. Figure 3 illustrates the dynamics of the wavefunction in a periodic field, showing the amplitudes of the different grid points while omitting those which are removed by the reprojection process for four values

of  $t$ . For an initial wavepacket starting at the origin, the wavefunction starts very localised before spreading starting from the high and low momenta points. The wavefunction then spreads more in the region where the momenta of the grid points are close to zero and a substantial portion of the wavefunction begins motion in an elliptical orbit around the origin as it interacts with the external field. This motion illustrates how the wavefunction loses some amplitude at the edges of the grid when the external field is at maxima or minima, and as such shows that during propagation a part of the wavefunction irreversibly leaves the dynamically important part of the phase space. It can be seen that the orbit travelled by this portion of the wavefunction differs from that of the classical motion because without reprojection the basis coherent states guided by Hamilton's equations (Eq. 15) move quickly away from the most important region around the elliptical orbit, as can be inferred from the motion of the trajectories shown in

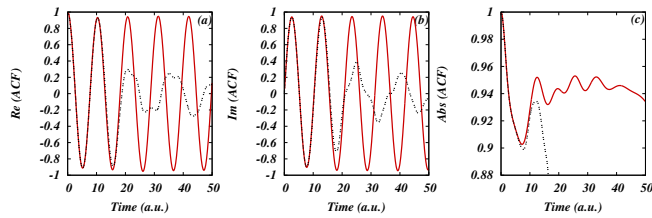


FIG. 4. Panes (a-c) give the real, imaginary and absolute values respectively of the ACFs when no reprojection is carried out on the wavefunction. Here the black dashed line is the CCS result and the red solid line is the result from the TDSE solver.

figure 1.

The efficacy of the reprojection technique can be determined by the auto-correlation function (ACF) which, unlike some other measures, is sensitive to changes over the entire wavefunction. When reprojection is not used the coupling between the coherent states is quickly lost. This results in the ACF decaying in both the real and imaginary parts as is shown in figure 4. With reprojection however, the coupling is maintained and although some information is lost at the edges of the grid the wavefunction still remains valid, as is shown in figure 5(a), which shows the absolute value of the

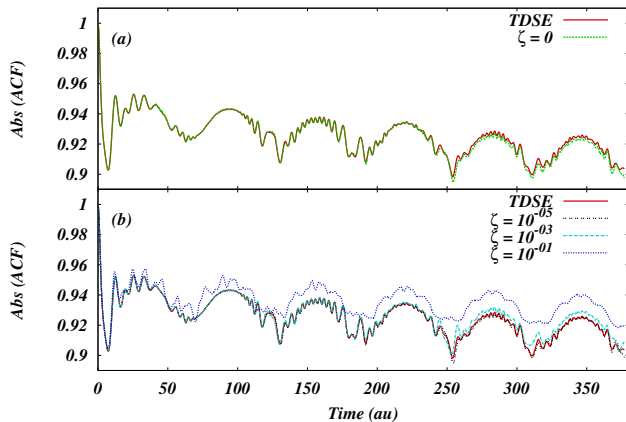


FIG. 5. Pane (a) gives comparison between the absolute values of the auto-correlation functions produced by the TDSE solver and the CCS method with  $\zeta = 0$ , showing near total agreement. Pane (b) gives the comparison between the absolute values of the auto-correlation functions produced by the TDSE solver and the CCS method for the first few values of the basis threshold parameter. It can be seen that the ACF for  $\zeta = 10^{-1}$  shows visible differences compared to the TDSE solver plot, but for values of  $\zeta \leq 10^{-3}$  the ACF begins to converge well towards the TDSE result, close enough that values for  $\zeta = 10^{-5}$  agrees almost exactly with the TDSE solver plot. Reprojection is carried out at every  $\tau = 1a.u.$  and the intensity of the external field is set at  $\mathcal{E}_0 = 0.1$  with a frequency of  $\omega_0 = 0.05$  for both comparisons. In all cases the wavepacket initially starts at  $(q,p) = (0,0)$ .

$\zeta$	$\Delta$	$N_{final}$	% speed-up
0	1.75	1601	-
$1 \times 10^{-10}$	1.75	1547	11.27
$1 \times 10^{-8}$	1.75	1521	16.04
$1 \times 10^{-6}$	1.75	1427	34.67
$1 \times 10^{-5}$	1.74	1196	61.56
$1 \times 10^{-4}$	1.71	715	89.23
$1 \times 10^{-3}$	1.59	328	98.44
$1 \times 10^{-2}$	1.28	39	99.88
$1 \times 10^{-1}$	1.00	15	99.99

TABLE I. Table of the parameters for the different wavefunctions. The grid parameter  $\Delta$  shows how the density of the grid increases as the basis threshold parameter increases, and the link between the computational expense and the number of basis functions can be clearly seen.

ACF for both the TDSE solver and the CCS method with  $\zeta = 0$ . As the two auto-correlation functions are in almost complete agreement this confirms the efficacy of the basic re-projection procedure. For other values of the basis threshold parameter the agreement between the plots varies.

For the higher values of  $\zeta$  there are noticeable discrepancies (figure 5(b)), however for values of  $\zeta \leq 10^{-3}$ , the plots converge towards the TDSE solver calculation result. Indeed, the ACF for  $\zeta = 10^{-5}$  is virtually indistinguishable from the TDSE result, and it can be seen from this and from table I that using  $\zeta_{MEC} = 10^{-5}$  is sufficient for accurate calculation of the ACF of the system while also reducing the computational expense of the simulation by over 50%. Even a very cheap calculation with the threshold parameter  $\zeta = 10^{-3}$ , which reduces computational cost by 98.4%, produces a result which is in good agreement with the benchmark for most of the propagation time.

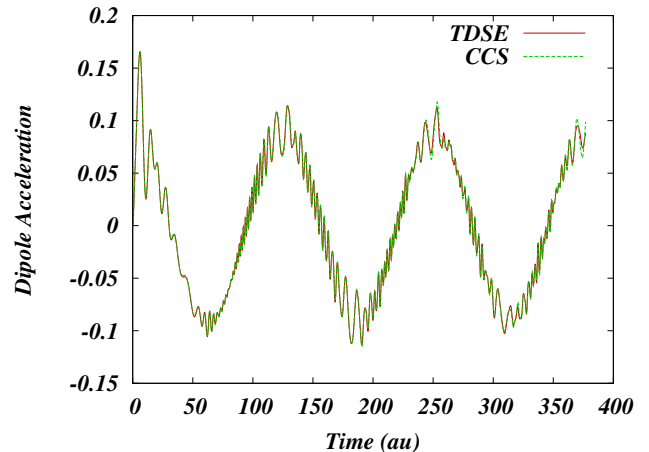


FIG. 6. Comparison between dipole acceleration graphs for the  $\zeta = \zeta_{MEC}$  CCS calculated wavefunction and the TDSE calculated plot

As mentioned earlier, the HHG spectrum is found by taking the Fourier transform of the dipole moment  $d(t)$ , which is calculated here in acceleration form so as to better probe the core. The plot of the dipole acceleration is given in figure 6, comparing the TDSE and CCS dipole accelerations, with the CCS plot calculated with  $\zeta = \zeta_{MEC}$ . The dipole acceleration exhibits a series of high-frequency oscillations. These oscillations, together with spatial localisation are responsible for the HHG plateau. Similar oscillations have also been identified and discussed in previous publications using TDSE computations [58] and the HK propagator [59] for cases where an initial wavepacket starts far from the core, and have been associated with the interference between different types of electron trajectories. The oscillations have also been studied in a different context, namely the adiabatic approximation [60, 61] and Bohmian trajectories [62, 63].

The extent to which the plots agree is good, being almost identical until the very end of the third oscillation of the cosine field. This agreement persists in the HHG spectrum. Figure 7 shows the HHG spectrum obtained from the TDSE solver compared against that from the CCS method for various values of the basis threshold parameter. The first panel shows the HHG spectrum for  $\zeta = 10^{-1}$ , and as can be seen the comparison with the TDSE solver generated spectrum is not very good, showing differences in the overall intensity in the region between around  $25\omega_0$  and the cut-off, disagreements with the positions of many of the peaks in the spectrum and fluctuations after the cut-off point which could confuse the position of the cut-off. The second panel is an improvement on this, using  $\zeta = 10^{-3}$ . This gives a much better agreement in the overall intensities over the spectrum, and much better agreement in the peak positions, however shows fluctuations after the cutoff which are not present in the TDSE solver spectrum. The third panel gives the spectrum for  $\zeta = \zeta_{MEC}$ , and it can be seen that there are few differences between this spectrum and that in the fourth panel where  $\zeta = 0$ , indeed despite the smaller basis set the HHG spectrum when  $\zeta = \zeta_{MEC}$  is virtually unchanged from the  $\zeta = 0$  spectrum. In both the third and fourth panels the spectra generated by the CCS calculation show excellent agreement with that of the TDSE solver, exhibiting the cut-off and plateau in the correct regions and agreeing almost completely for the features of the spectrum, although some low amplitude fluctuations after the cut-off are still present due to numerical effects.

#### IV. CONCLUSIONS

In summary, the work presented in this article demonstrates the ability of the Coupled Coherent States (CCS) method to accurately simulate strong field phenomena

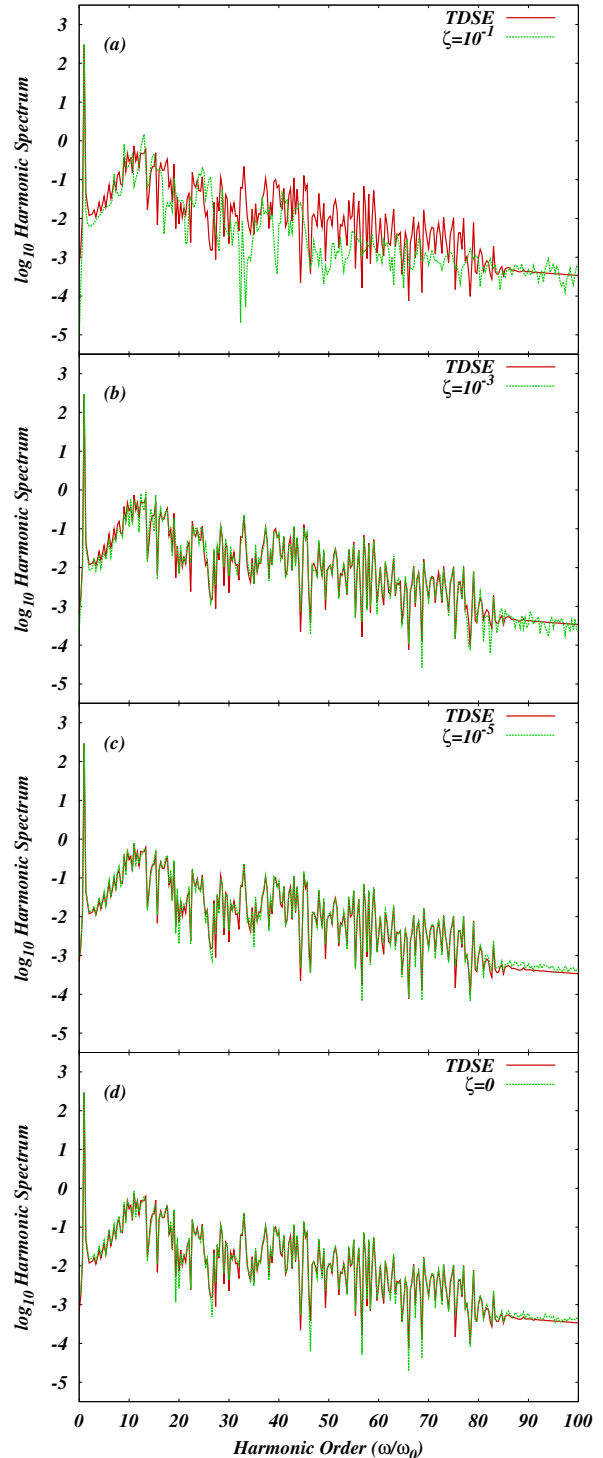


FIG. 7. Comparisons of HHG spectra generated by the TDSE solver and those generated by the CCS method with various basis threshold parameter values, with  $\zeta = 10^{-1}$  in panel (a),  $\zeta = 10^{-3}$  in panel (b),  $\zeta = \zeta_{MEC}$  in panel (c) and  $\zeta = 0$  in panel (d).

such as the HHG spectrum of an electron in a laser field in one dimension. It has been shown that when using a large grid of coherent states as a basis, trajectory decoupling can be prevented through re-projection of the wavefunction and computational cost can be reduced by adaptively reducing the basis set size. This has allowed the method to account for wavefunctions which spread out to cover large areas in phase space without being prohibitively computationally expensive. The re-projection of the wavefunction relies on a large regular grid which scales exponentially with the number of degrees of freedom of a system. Since only a small part of the grid is kept during the re-projection however, the cost of the computation can be greatly reduced, with very accurate results obtained with a  $> 60\%$  speedup, and a good reproduction of the majority of the spectrum with a  $> 98\%$  speedup. The CCS method is an accurate simulation technique, which allows numerical experiments in realistic and complicated quantum systems. By representing quantum dynamics in phase space it allows the visualisation of the trajectories of quantum wavefunctions. In the particular case of a single electron in a periodic electric field it is shown that the wavefunction is localised around an elliptical

orbit which however is non-classical and needs to be understood.

Furthermore, for multidimensional systems we expect the reduction of the grid to play even greater role than here, hence further reducing computational cost. In addition the CCS method using the re-projection scheme can be used in the future to treat only the most important degrees of freedom in a system with the rest treated by a single Gaussian, in the spirit of the multiconfigurational Ehrenfest method [45–47], which will be the subject of future work aiming at more challenging multi-electron systems.

## V. ACKNOWLEDGEMENTS

This work was funded by The University of Leeds School of Chemistry DTG programme, the UK EPSRC (Grants EP/J019143/1 and EP/J019240/1) and the CSC/BIS (China-UK Studentship for Excellence). The authors would like to thank Adam Kirrander and Bradley Augustein for useful discussions.

- 
- [1] N. A. Papadogiannis, B. Witzel, C. Kalpouzos, and D. Charalambidis, *Phys. Rev. Lett.* **83**, 4289 (1999).
  - [2] R. A. Bartels, A. Paul, H. Green, H. C. Kapteyn, M. M. Murnane, S. Backus, I. P. Christov, Y. Liu, D. Attwood, and C. Jacobsen, *Science* **297**, 376 (2002).
  - [3] Z. Zeng, Y. Cheng, X. Song, R. Li, and Z. Xu, *Phys. Rev. Lett.* **98**, 203901 (2007).
  - [4] Y. Oishi, M. Kaku, A. Suda, F. Kannari, and K. Midorikawa, *Opt. Express* **14**, 7230 (2006).
  - [5] V. S. Yakovlev, M. Ivanov, and F. Krausz, *Opt. Express* **15**, 15351 (2007).
  - [6] T. Pfeifer, A. Jullien, M. J. Abel, P. M. Nagel, L. Gallmann, D. M. Neumark, and S. R. Leone, *Opt. Express* **15**, 17120 (2007).
  - [7] M. Klaiber, K. Z. Hatsagortsyan, C. Müller, and C. H. Keitel, *Opt. Lett.* **33**, 411 (2008).
  - [8] A. Baltuska, T. Udem, M. Uiberacker, M. Hentschel, E. Goulielmakis, C. Gohle, R. Holzwarth, V. S. Yakovlev, A. Scrinzi, T. W. Hansch, and F. Krausz, *Nature* **421**, 611 (2003).
  - [9] G. Sansone, E. Benedetti, F. Calegari, C. Vozzi, L. Avaldi, R. Flammini, L. Poletto, P. Villoresi, C. Altucci, R. Velotta, S. Stagira, S. De Silvestri, and M. Nisoli, *Science* **314**, 443 (2006).
  - [10] E. Goulielmakis, M. Schultze, M. Hofstetter, V. S. Yakovlev, J. Gagnon, M. Uiberacker, A. L. Aquila, E. M. Gullikson, D. T. Attwood, R. Kienberger, F. Krausz, and U. Kleineberg, *Science* **320**, 1614 (2008).
  - [11] S. Haessler, J. Caillat, W. Boutu, C. Giovanetti-Teixeira, T. Ruchon, T. Auguste, Z. Diveki, P. Breger, A. Maquet, B. Carre, R. Taieb, and P. Salieres, *Nat. Phys.* **6**, 200 (2010).
  - [12] J. Itatani, J. Levesque, D. Zeidler, H. Niikura, H. Pepin, J. C. Kieffer, P. B. Corkum, and D. M. Villeneuve, *Nature* **432**, 867 (2004).
  - [13] P. B. Corkum, *Phys. Rev. Lett.* **71**, 1994 (1993).
  - [14] J. L. Krause, K. J. Schafer, and K. C. Kulander, *Phys. Rev. Lett.* **68**, 3535 (1992).
  - [15] K. J. Schafer, B. Yang, L. F. DiMauro, and K. C. Kulander, *Phys. Rev. Lett.* **70**, 1599 (1993).
  - [16] K. C. Kulander, K. J. Schafer, and J. L. Krause, *Superintense Laser-Atom Physics, NATO Advanced Study Institute Series B: Physics*, edited by B. Piraux, A. L’Huillier, and K. Rzazewski, Vol. 316 (Plenum, New York, 1993) p. 95.
  - [17] M. Lewenstein, P. Balcou, M. Y. Ivanov, A. L’Huillier, and P. B. Corkum, *Phys. Rev. A* **49**, 2117 (1994).
  - [18] S. Baier, C. Ruiz, L. Plaja, and A. Becker, *Phys. Rev. A* **74**, 033405 (2006).
  - [19] S. Baier, C. Ruiz, L. Plaja, and A. Becker, *Laser Physics* **17**, 358 (2007).
  - [20] F. Lepine, M. Y. Ivanov, and M. J. J. Vrakking, *Nat. Photon.* **8**, 195 (2014).
  - [21] L. V. Keldysh, *Sov. Phys. JETP* **20**, 1307 (1965).
  - [22] F. H. M. Faisal, *J. Phys. B* **6**, L89 (1973).
  - [23] H. R. Reiss, *Phys. Rev. A* **22**, 1786 (1980).
  - [24] T.-M. Yan, S. V. Popruzhenko, M. J. J. Vrakking, and D. Bauer, *Phys. Rev. Lett.* **105**, 253002 (2010).
  - [25] W. Quan, Z. Lin, M. Wu, H. Kang, H. Liu, X. Liu, J. Chen, J. Liu, X. T. He, S. G. Chen, H. Xiong, L. Guo, H. Xu, Y. Fu, Y. Cheng, and Z. Z. Xu, *Phys. Rev. Lett.* **103**, 093001 (2009).
  - [26] C. I. Blaga, F. Catoire, P. Colosimo, G. G. Paulus, H. G. Muller, P. Agostini, and L. F. DiMauro, *Nat. Phys.* **5**, 335 (2008).

- [27] D. A. Telnov and S.-I. Chu, *Phys. Rev. A* **83**, 063406 (2011).
- [28] D. G. Arbó, S. Yoshida, E. Persson, K. I. Dimitriou, and J. Burgdörfer, *Phys. Rev. Lett.* **96**, 143003 (2006).
- [29] A. Rudenko, K. Zrost, C. D. Schröter, V. L. B. de Jesus, B. Feuerstein, R. Moshhammer, and J. Ullrich, *J. Phys. B* **37**, L407 (2004).
- [30] F. Mauger, C. Chandre, and T. Uzer, *Phys. Rev. Lett.* **105**, 083002 (2010).
- [31] A. Kamor, F. Mauger, C. Chandre, and T. Uzer, *Phys. Rev. Lett.* **110**, 253002 (2013).
- [32] S. V. Popruzhenko, G. G. Paulus, and D. Bauer, *Phys. Rev. A* **77**, 053409 (2008).
- [33] O. Smirnova, M. Spanner, and M. Ivanov, *J. Phys. B* **39**, S307 (2006).
- [34] O. Smirnova, M. Spanner, and M. Ivanov, *Phys. Rev. A* **77**, 033407 (2008).
- [35] D. V. Shalashilin and M. S. Child, *Chem. Phys.* **304**, 103 (2004).
- [36] D. V. Shalashilin and M. S. Child, *J. Chem. Phys.* **122**, 224108 (2005).
- [37] P. A. J. Sherratt, D. V. Shalashilin, and M. S. Child, *Chem. Phys.* **322**, 127 (2006).
- [38] D. V. Shalashilin and M. S. Child, *J. Chem. Phys.* **128**, 054102 (2008).
- [39] D. V. Shalashilin, M. S. Child, and A. Kirrander, *Chem. Phys.* **347**, 257 (2008).
- [40] D. V. Shalashilin and M. S. Child, *J. Chem. Phys.* **114**, 9296 (2001).
- [41] A. Kirrander and D. V. Shalashilin, *Phys. Rev. A* **84**, 033406 (2011).
- [42] C. Zagoya, J. Wu, M. Ronto, D. Shalashilin, and C. Figueira de Morisson Faria, “Quantum And Semiclassical Phase-Space Dynamics Of A Wave Packet In Strong Fields Using Initial-Value Representations,” (2014), in Press.
- [43] A. Perelomov, *Generalized Coherent States and Their Applications* (Springer-Verlag, 1986).
- [44] M. S. Child and D. V. Shalashilin, *J. Chem. Phys.* **118**, 2061 (2003).
- [45] M. Ronto, A. Grigolo, and D. Shalashilin, “A multi-layer approach to the coupled coherent states method,” (2014), (Submitted).
- [46] D. V. Shalashilin, *J. Chem. Phys.* **130**, 244101 (2009).
- [47] D. V. Shalashilin, *J. Chem. Phys.* **132**, 244111 (2010).
- [48] K. Saita and D. V. Shalashilin, *J. Chem. Phys.* **137**, 22A506 (2012).
- [49] K. Saita, M. G. D. Nix, and D. V. Shalashilin, *Phys. Chem. Chem. Phys.* **15**, 16227 (2013).
- [50] D. V. Makhov, W. J. Glover, T. J. Martinez, and D. V. Shalashilin, *J. Chem. Phys.* **141**, 054110 (2014).
- [51] K. Burnett, V. C. Reed, J. Cooper, and P. L. Knight, *Phys. Rev. A* **45**, 3347 (1992).
- [52] J. L. Krause, K. J. Schafer, and K. C. Kulander, *Phys. Rev. A* **45**, 4998 (1992).
- [53] D. V. Shalashilin and B. Jackson, *Chem. Phys. Lett.* **318**, 305 (2000).
- [54] J. C. Burant and V. S. Batista, *J. Chem. Phys.* **116**, 2748 (2002).
- [55] D. Huber and E. J. Heller, *J. Chem. Phys.* **89**, 4752 (1988).
- [56] D. Huber and E. J. Heller, *J. Chem. Phys.* **87**, 5302 (1987).
- [57] N. Takemoto, A. Shimshovitz, and D. J. Tannor, *J. Chem. Phys.* **137**, 011102 (2012).
- [58] M. Protopapas, D. G. Lappas, C. H. Keitel, and P. L. Knight, *Phys. Rev. A* **53**, R2933 (1996).
- [59] C. Zagoya, C.-M. Goletz, F. Grossmann, and J.-M. Rost, *Phys. Rev. A* **85**, 041401 (2012).
- [60] O. I. Tolstikhin and T. Morishita, *Phys. Rev. A* **86**, 043417 (2012).
- [61] Y. Okajima, O. I. Tolstikhin, and T. Morishita, *Phys. Rev. A* **85**, 063406 (2012).
- [62] J. Wu, B. B. Augstein, and C. Figueira de Morisson Faria, *Phys. Rev. A* **88**, 023415 (2013).
- [63] J. Wu, B. B. Augstein, and C. Figueira de Morisson Faria, *Phys. Rev. A* **88**, 063416 (2013).